

Prediction of a Giant Magnetoelectric Cross-Caloric Effect Around a Tetracritical Point in Multiferroic SrMnO₃

Alexander Edström and Claude Ederer

Materials Theory, ETH Zürich, Wolfgang-Pauli-Strasse 27, 8093 Zürich, Switzerland

We study the magnetoelectric and electrocaloric response of strain-engineered, multiferroic SrMnO₃, using a phenomenological Landau theory with all parameters obtained from *first-principles*-based calculations. This allows to make realistic and materials-specific predictions about the magnitude of the corresponding effects. We find that in the vicinity of a tetracritical point, where magnetic and ferroelectric phase boundaries intersect, an electric field has a huge effect on the antiferromagnetic order, corresponding to a magnetoelectric response several orders of magnitude larger than in conventional linear magnetoelectrics. Furthermore, the strong magnetoelectric coupling leads to a magnetic, cross-caloric contribution to the electrocaloric effect, which increases the overall caloric response by about 60%. This opens up new potential applications of antiferromagnetic multiferroics in the context of environmentally friendly solid state cooling technologies.

Introduction - Caloric effects in ferroic materials, where application/removal of external fields (magnetic, electric, or stress) can result in significant temperature changes, potentially allow for the development of clean and energy-efficient cooling technologies^{1,2}. More recently, there has been growing interest in so-called multicaloric effects^{3,4}, where more than one type of caloric effect can occur simultaneously, possibly allowing to further optimize the total caloric response. The thermodynamic theory of multicaloric effects has been discussed in some detail⁵⁻⁷. However, most specific studies have been focusing on combining either electrocaloric or magnetocaloric with elastocaloric effects, thereby using applied stress or strain as an additional control parameter to enhance the overall caloric response⁸⁻¹⁰ and/or to reduce irreversibility problems¹¹⁻¹⁴. Multicaloric effects in (single phase) materials combining magnetic and ferroelectric (FE) order, meanwhile, have remained relatively unexplored^{2,3}, perhaps due to challenges in finding suitable materials.

Multiferroic materials with coexisting magnetic and FE orders have received much attention, not only because of a broad fundamental interest, but also due to promises of technological applications^{15,16}. Often, however, their practical usefulness is hindered by low ordering temperatures or weak magnetoelectric (ME) coupling. Additionally, most magnetic ferroelectrics are in fact antiferromagnetic (AFM), which restricts their potential applications, since the AFM order does not couple to a homogeneous magnetic field. Here we show that an AFM multiferroic can, nevertheless, exhibit a very strong cross-caloric magnetic contribution to the electrocaloric effect (ECE)¹⁷.

Since caloric effects are generally largest near the relevant phase transitions, a strong cross-caloric effect can be expected near a so-called *tetracritical point* (TCP)¹⁸, where the critical temperatures of the two phase transitions coincide. Such a TCP has recently been predicted to occur in strained SrMnO₃¹⁹; its existence can also be inferred from previous theoretical²⁰ and experimental²¹⁻²³ work. While perovskite structure bulk SrMnO₃

is a cubic paraelectric G-type antiferromagnet²⁴, it develops a FE distortion under tensile epitaxial strain²⁰⁻²³. Thereby, the FE critical temperature increases strongly with strain¹⁹, while the AFM Néel temperature is less affected, resulting in an intersection of the FE and AFM phase boundaries at a certain strain value, and thus a TCP. Furthermore, since the Mn cation carries the magnetic moment and also takes part in the FE distortion, SrMnO₃ is expected to exhibit strong ME coupling, which is also implied by recent studies reporting a particularly strong spin-phonon coupling in this material^{25,26}.

In this work, we explore ME coupling effects and cross-caloric response in SrMnO₃ by constructing a Landau-type theoretical model considering all relevant magnetic and ferroelectric order parameters. We extract all parameters entering the free energy from *first principles*-based calculations, thus allowing for a realistic materials-specific description. We then apply the model to study ME coupling phenomena around the multiferroic TCP in SrMnO₃. We show that an applied electric field has a strong effect on the AFM order, shifting its critical temperature and increasing the corresponding order parameter, thereby drastically changing the entropy of the magnetic sub-system. This results in a huge magnetic cross-caloric contribution to the ECE, which is increased by about 60% due to the ME coupling.

Methods - SrMnO₃ under epitaxial strain is predicted to show a number of different magnetic phases, including G, C and A-type AFM²⁷, and possibly also ferromagnetic (FM) at large strains (near 5%)^{19,20}. Furthermore, in the cubic structure, there are three different degenerate \mathbf{q} -vectors corresponding to each of the A-type and C-type AFM orders. When the cubic symmetry is broken this degeneracy is also broken. Thus, we consider eight magnetic order parameters: FM [$\mathbf{q} = (0, 0, 0)$], G [$\mathbf{q} = (1, 1, 1)$], A [$\mathbf{q} = (0, 0, 1)$ or $\mathbf{q} = (0, 1, 0)$ or $\mathbf{q} = (1, 0, 0)$] and C [$\mathbf{q} = (1, 1, 0)$ or $\mathbf{q} = (1, 0, 1)$ or $\mathbf{q} = (0, 1, 1)$], where the reciprocal space vectors are given in units of π divided by the real space lattice constant along that direction. This includes all magnetic orders that have been reported to appear in SrMnO₃¹⁹. Each of these magnetic order

parameters can couple to the polar order P that emerges

under strain. Hence, we consider a Landau free energy of the form

$$\mathcal{F}_q = \frac{1}{2}a_P(T, \eta)P^2 + \frac{b_P}{4}P^4 + \frac{1}{2}a_q(T, \eta)M_q^2 + \frac{b_q}{4}M_q^4 + \frac{\lambda_q(\eta)}{2}M_q^2P^2 - EP, \quad (1)$$

for each magnetic order parameter $M_q = \frac{1}{N} \sum_i^N e^{i\mathbf{q}\cdot\mathbf{R}_i} \langle S_i \rangle$, where $\langle S_i \rangle$ is the thermodynamic average of the normalized spin at site \mathbf{R}_i , projected on the spin-quantization axis, and N is the number of spins. The strain and temperature dependence enters in the second order coefficients as $a_P = \alpha_P(T - T_0^P) + c_P\eta$ and $a_q = \alpha_q(T - T_0^q) + c_q\eta$. At each strain η , temperature T , and electric field E , the free energy \mathcal{F}_q is minimized with respect to P and M_q , and the free energy is determined from $\mathcal{F} = \min_q \mathcal{F}_q$. The q which corresponds to the lowest free energy defines the equilibrium magnetic phase at that point in the phase diagram.

All parameters in Eq. (1) were determined from total energy calculations using density functional theory (DFT) and DFT-based effective Hamiltonian simulations^{19,28}. Specifically, the magnetic parameters were obtained by mapping DFT total energy calculations on a Heisenberg Hamiltonian and extracting exchange interaction parameters. By calculating exchange interactions as functions of strain, the coupling between strain and magnetism was obtained, while exchange interactions evaluated with FE structural distortions allowed the determination of the biquadratic magnetoelectric coupling coefficients λ_q . The purely ferroelectric parameters are determined from the strain-dependent transition temperature and saturation polarization obtained from first-principles-based effective Hamiltonians¹⁹, and from DFT calculated elastic/electro-strictive parameters.

Results - We first consider the case without ME coupling and zero applied field, i.e., $\lambda_q = 0$ and $E = 0$, and minimize the free energy in Eq. (1) with respect to the various order parameters for different temperatures and strains in the range $0 \leq \eta \leq 5\%$. Identifying the phases with the lowest free energy for each strain and temperature results in the phase diagram shown in Fig. 1, which agrees well with the one from our previous study using microscopic first-principles-based Hamiltonians¹⁹. For small T and η , there is a G-type AFM paraelectric (PE) phase, while at approximately 2% strain there is a transition into a FE region and also a change to C-type $[\mathbf{q} = (1, 0, 1)]$ AFM order. For large strain and low temperatures, an A-type $[\mathbf{q} = (0, 0, 1)]$ AFM FE region appears. In the following C and A-type AFM always refer to \mathbf{q} -vectors $(1, 0, 1)$ and $(0, 0, 1)$, since these are the only ones that appear in the phase diagram. We note that the ferromagnetism that has been predicted for large strains is only stabilized due to its coupling to the FE order¹⁹, which at this point is not yet included in our free energy. Most notably, the phase diagram in Fig. 1 reveals

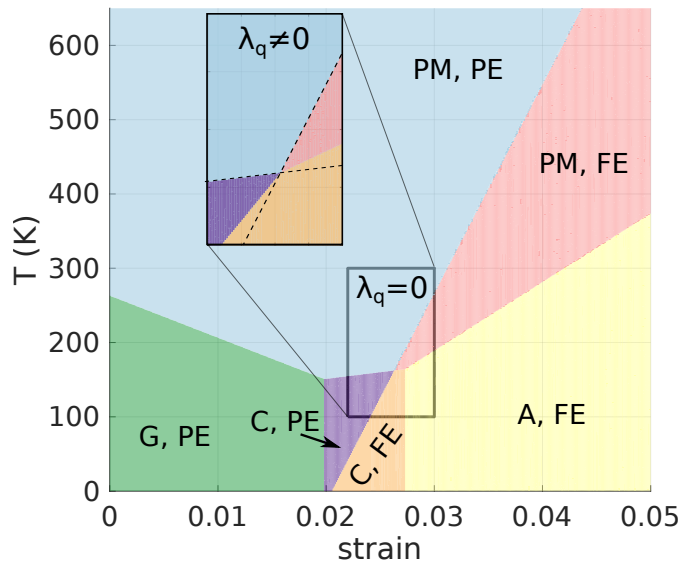


Figure 1. Ferroic phase diagram of SrMnO₃ at zero applied field obtained within our Landau theory for the case without ME coupling ($\lambda_q = 0$). The inset shows the effect of non-zero ME coupling on the region around the TCP. The dashed lines in the inset indicate the FE-PE and the C-paramagnetic (PM) phase boundaries with $\lambda_q = 0$.

a TCP where the magnetic and FE critical temperatures coincide within the region with C-type AFM order at $\eta_{\text{tcp}} = 2.63\%$ and $T_{\text{tcp}} = 162$ K.

Next, we evaluate the strain-dependent ME coupling parameters, λ_q , by computing magnetic exchange interactions as functions of the FE displacements for different strains. As shown in the supplementary material²⁸, it turns out that the lowest order biquadratic coupling in Eq. (1) is insufficient to describe the variation of the exchange couplings for large polarization, which occurs in the region of the phase diagram with large strain and low temperatures. A satisfactory description of this region would require coupling terms of higher order in P , which, however, would require additional higher order terms to guarantee stable, physical solutions, and thus more parameters in the free energy. In the following, we therefore focus on the part of the phase diagram which is most interesting in the present context, i.e., the region around the TCP, where both order parameters are small²⁹.

For the C-type order relevant around the TCP, we find a negative ME coupling, which varies relatively weakly

with strain. We point out that, previously, a positive ME coupling coefficient λ_G has been found for cubic $\text{Sr}_{1-x}\text{Ba}_x\text{MnO}_3$ ^{30,31}, meaning that G-type AFM order and ferroelectricity couple unfavorably. This is indeed consistent with our results²⁸. However, we also find that the coupling coefficients differ for different types of magnetic order and, furthermore, are strongly strain-dependent.

The zero field phase diagram for the region $2.2\% \leq \eta \leq 3.0\%$ and $100 \text{ K} \leq T \leq 300 \text{ K}$, now including ME coupling, is shown in the inset of Fig. 1. One drastic effect of the coupling is that it eliminates the A-type AFM region from the phase diagram. This is because λ_A is found to be strongly positive and since A-type order only appears in the FE region, it is highly unfavored by the coupling, while C-type is favored. In contrast, the coupling does not alter the position of the TCP, since both M_C and P , and thus the effect of the coupling term, vanish at this point. Away from the TCP, the upper of the two ordering temperatures also remains unaltered, while the lower one is increased by the negative ME coupling. This can also be seen from Figs. 2(a) and (b), which show the temperature dependence of the FE polarization P and the C-AFM order parameter M_C , both with (black) and without (blue) ME coupling, for three different strain values. At $\eta = 2.80\%$ (where $T_c^C < T_c^P$), T_c^P is unaffected, while the magnetic order is changed from A-type to C-type with an increase in ordering temperature from $T_c^A = 170 \text{ K}$ to $T_c^C = 174 \text{ K}$. In addition, the polarization is unaffected by the coupling at temperatures above $T_c^C = 174 \text{ K}$, while the coupling enhances the polarization at lower temperatures, producing a kink in $P(T)$ at T_c^C . The analogous behavior, but with the roles of P and M_C exchanged, is observed at $\eta = 2.50\%$ (where $T_c^C > T_c^P$). Here, the coupling does not alter T_c^M , while it shifts T_c^P from 127 K to 139 K , resulting in a kink in $M_C(T)$ at $T_c^P = 139 \text{ K}$. On the other hand, at $\eta_{\text{tcp}} = 2.63\%$, the coinciding critical temperatures are unaltered by the coupling term. However, below $T_{\text{tcp}} = 162 \text{ K}$, both order parameters are enhanced compared to the case with $\lambda_q = 0$. This behavior is consistent with the general phenomenological theory outlined in Ref. [7], where it was also shown that both transitions remain second order if $\lambda_q^2 < b_q b_p$ (or if $\lambda_q > 0$). According to our results this condition is fulfilled for every magnetic order and strain considered.

The zero-field electric susceptibility $\chi_E = \frac{dP}{dE}|_{E=0}$ (for the case with ME coupling), is also plotted in Fig. 2(a) (red, right y -axis). As expected, this susceptibility diverges at the FE transitions. Additionally, the magneto-electric susceptibility

$$\chi_{ME} = \left. \frac{dM_q}{dE} \right|_{E=0} = \begin{cases} 0, & \text{if } M_q = 0 \text{ or } P = 0 \\ -\frac{\lambda_q P}{b_q M_q} \chi_E, & \text{if } M_q \neq 0 \text{ and } P \neq 0 \end{cases} \quad (2)$$

is plotted in Fig. 2(b) (red, right y -axis). This quantity describes the magnetic response to an applied electric field and is non-zero only in the multiferroic regions of the

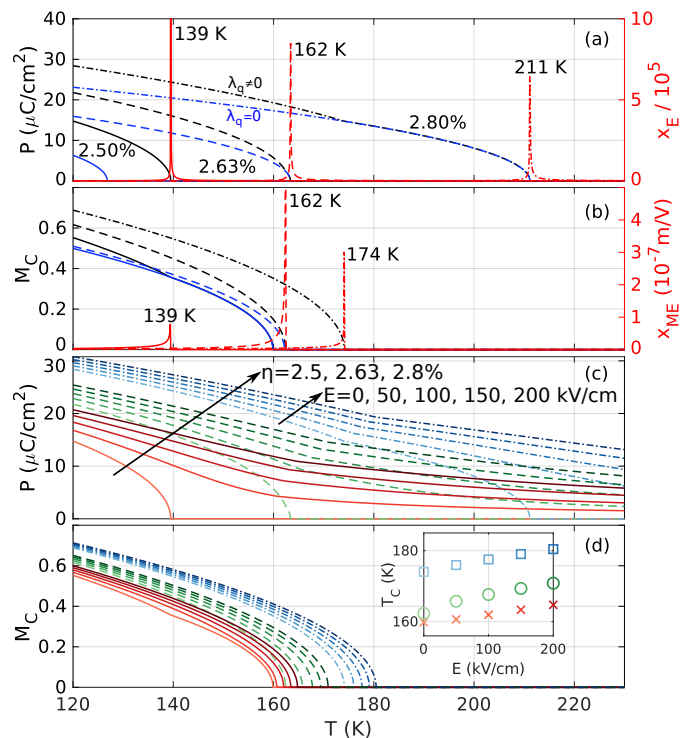


Figure 2. (a) and (b): Order parameters (black, left) and susceptibilities (red, right) as functions of temperature for the three strains of 2.5% (solid line), 2.63% (dashed line) and 2.8% (dashed dotted line). (a) shows the electric polarization and electric susceptibility, while (b) shows the magnetic order parameter and ME susceptibility. The order parameters for zero ME coupling are shown in blue. (c) and (d): Temperature dependence of FE (c) and magnetic (d) order parameters for strains of 2.5% (red solid lines), 2.63% (green dashed lines) and 2.8% (blue dashed dotted lines) with applied electric fields of 0, 50, 100, 150 and 200 kV/cm. The darker colors correspond to larger fields. The inset in (d) shows the magnetic transition temperature as function of electric field, with color coding corresponding to the main plot.

phase diagram, i.e., where both magnetic and FE order parameters are non-zero. The ME susceptibility then diverges at the lower of the two transition temperatures, either because χ_E diverges if the FE transition is lower, or because $M_q \rightarrow 0$ if the magnetic transition is lower. Thus, χ_{ME} diverges at $T_c^P = 139 \text{ K}$ for $\eta = 2.50\%$, at $T_c^M = T_c^P = 162 \text{ K}$ for $\eta_{\text{tcp}} = 2.63\%$, and at $T_c^M = 174 \text{ K}$ for $\eta = 2.80\%$. The divergence is particularly pronounced at η_{tcp} , where χ_E diverges simultaneously as $M_q \rightarrow 0$, causing χ_{ME} to diverge as $(T_c - T)^{-1}$ instead of $(T_c - T)^{-1/2}$ when the relevant critical temperature T_c is approached from below³².

We now discuss the effect of applying a finite electric field. In Fig. 2(c)-(d), the FE and magnetic order parameters are plotted as functions of temperature for the previously discussed strain values and various applied electric fields. As expected, an electric field induces a finite electric polarization at all temperatures, which

however, decreases towards high T , and thus removes the second order FE transition. The effect on the magnetic order parameter is markedly different. While the electric field enhances also M_C , due to the negative sign of λ_C , the magnetic order parameter still shows a second order transition, and is identically zero above the corresponding transition temperature. The magnetic transition temperature is, however, field dependent and the inset of Fig. 2(d) shows T_c^C as a function of applied electric field. The increase in T_c^C with E appears close to linear, and an applied field of 100 keV/cm² increases T_c^C by 2.1 K for $\eta = 2.5\%$, by 5.3 K for $\eta = 2.63\%$, and by 3.5 K for $\eta = 2.8\%$. The largest effect of the electric field on T_c^C is thus found at η_{tcp} .

We note that SrMnO₃ is not a linear ME material. Nevertheless, in order to get a better idea of the magnitude of the electric field effect on M_C , one can see from Fig. 2(d) that an electric field of 50 keV/cm alters M_C by about 0.15 at the TCP. Considering a Mn magnetic moment of $3\mu_B$, one can estimate an effective ME coefficient of $\alpha_{\text{eff}} = \frac{\Delta M}{\Delta E} = 15 \cdot 10^{-3} \Omega^{-1}$, which is four orders of magnitude larger than that found in conventional linear magnetoelectrics such as Cr₂O₃^{33,34}.

Based on the electric field response of both FE and magnetic order parameters, we can now address the ECE in SrMnO₃. From the results presented so far, it is apparent that, due to the negative ME coupling coefficient, an applied electric field has an ordering tendency on both the FE and magnetic subsystems, and hence reduces the entropy in both. This will result in a magnetic contribution to the ECE, referred to as cross-caloric⁷. The caloric response is quantified by the isothermal entropy change under field application or removal. From the free energy in Eq. (1), the entropy at a given temperature and field E is $S(T, E) = -(\frac{\partial F}{\partial T})_E$, while the entropy change when increasing the field from 0 to E is $\Delta S(T, E) = S(T, E) - S(T, 0) = -\frac{1}{2}\alpha_P (P^2(T, E) - P^2(T, 0)) - \frac{1}{2}\alpha_q (M_q^2(T, E) - M_q^2(T, 0))$. Here, the first term is the usual ECE, while the second term is the magnetic contribution, i.e., the cross-caloric response.

Fig. 3(a)-(c) show the isothermal entropy change in SrMnO₃ as function of temperature for an applied field of 150 keV/cm, at the three representative strain values discussed previously ($\eta = 2.5\%$, $\eta = 2.63\%$, and $\eta = 2.8\%$). The total entropy change has been decomposed in magnetic and electric contributions and the ECE obtained without ME coupling ($\lambda_q = 0$) is also plotted as a black line. The total caloric response exhibits features (peaks and/or kinks) at all critical temperatures (with or without field). Generally, the electric contribution is non-zero at all temperatures and peaks at the zero field T_c^C . Below but near $T_c^C(E)$ it is enhanced compared to the case without ME coupling. For $\eta = 2.9\%$ this even leads to an additional small peak at $T_c^C(0)$. Hence, the ME coupling can enhance the ECE not only by adding the magnetic cross-caloric effect, but also by enhancing the electric part. The magnetic contribution vanishes above $T_c^C(E)$, but rises sharply between $T_c^C(E)$ and $T_c^C(0)$, peaking at

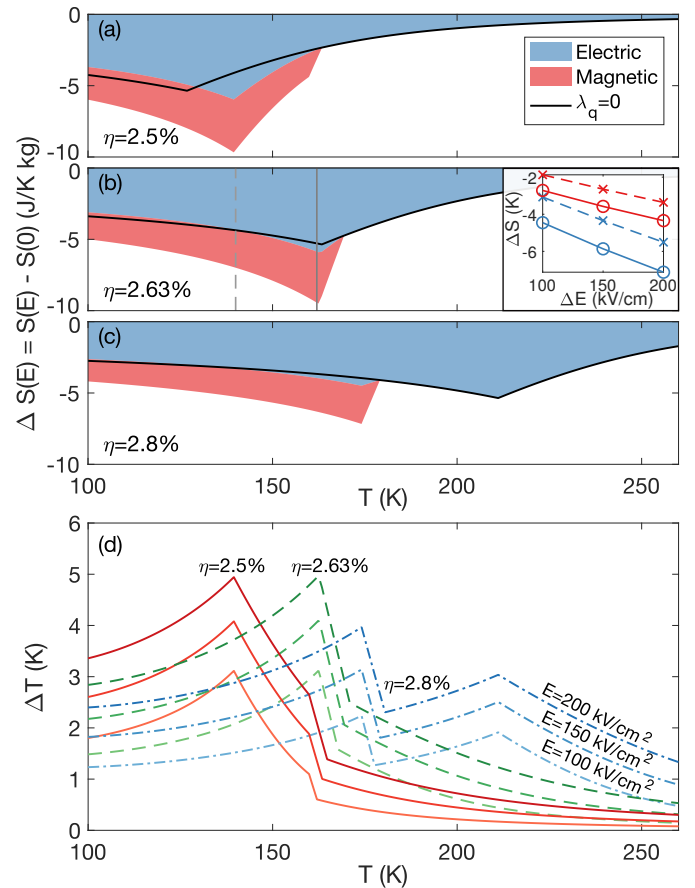


Figure 3. The ECE as function of temperature. (a)-(c) show the isothermal entropy change, as a field of 150 keV/cm is applied, for the three different strains of 2.5%, 2.63% and 2.8%, respectively, while (b) also contains an inset showing the field dependence at $T = 140$ K (dashed) and $T = 162$ K (solid). The total entropy change is decomposed into magnetic (red) and electric (blue) contributions. Additionally, the result occurring without ME coupling ($\lambda_q = 0$) is shown (black line). (d) shows an estimate of the adiabatic temperature change corresponding to the total isothermal entropy change for strains of 2.5%, 2.63% and 2.8%, and applied electric fields of 100, 150 or 200 keV/cm.

$T_c^C(0)$, then slowly decreases again towards lower T , except for the case of $\eta = 2.5\%$, where it actually peaks at T_c^P . This is related to the kink in $M_C(T)$ at this temperature for zero field (see Fig. 2(b)). The inset in Fig. 3(b) shows the magnetic and electric contributions to the entropy change at $\eta = 2.63\%$ and temperatures 140 K and 162 K, as functions of applied electric field, which illustrates an approximately linear increase in the magnitude of the entropy change with the field.

Most strikingly, at all three strains, the magnetic contribution reaches approximately 60% of the electric contribution, or more than a third of the total entropy change. This is a result of particular relevance, since it shows that the ME cross-caloric effect can significantly increase the caloric response suitable for solid state cool-

ing. Furthermore, the effect is of similar size for the three different strains, indicating that a very careful tuning of the two critical temperatures to coincide is not necessary. It is also interesting to note that, in the case of $\eta = 2.8\%$, the largest total ECE is not obtained at the FE phase transition, but at the magnetic one. This is because it is the lower temperature phase transition in this case and thus the two contributions add up, while at the FE transition the magnetic contribution vanishes.

Another instructive quantity to characterize caloric effects is the adiabatic temperature change ΔT , which can be estimated from the entropy change ΔS via the thermodynamic relation $dT = -\frac{T}{C}dS$, where C is the specific heat at constant field, without the contributions of the FE or magnetic degrees of freedom³⁵. We use this relation to estimate $\Delta T \approx -\frac{T}{C}\Delta S$, assuming that $\Delta T \ll T$ and that C varies negligibly over $[T, T + \Delta T]$. For C , we use the temperature dependent phonon specific heat, which we obtained for cubic SrMnO₃, from frozen phonon calculations in the harmonic approximation³⁶. This results in a double counting of the phonon modes responsible for ferroelectricity, which might slightly underestimate ΔT . The resulting ΔT is plotted in Fig. 3(d), for the same strains as in (a)-(c), and three different applied fields. The largest temperature changes, for $E = 200$ kV/cm, are about 5 K. This is of the order of magnitude needed to be technologically relevant and of similar size as the ECE found in high performing electrocaloric materials for similar field strengths². Although being estimates, the temperature changes in Fig. 3(d) show that multiferroic perovskite oxides can indeed be of potential technological relevance within the area of solid state cooling.

Summary and conclusions - We have used a Lan-

dau theory, allowing several magnetic order parameters to couple to a FE polarization, to study ME coupling phenomena around the TCP appearing in the strain-temperature phase diagram of SrMnO₃. Since all parameters entering the theory have been determined from *first principles* DFT-based calculations, realistic materials specific predictions can be made without experimental input. The ME coupling is found to be enhanced at the TCP and a huge response to electric fields is observed in the magnetic order parameter. Investigating the ECE, we find a large cross-caloric contribution due to the electric-field-induced magnetic entropy change, resulting in an increase of about 60% in the total caloric response. This provides a new way for greatly enhancing caloric effects for solid state cooling applications, by using multiferroic materials with coupled magnetic and electric order parameters. It also provides a unique example where AFM order in a multiferroic material can be of great practical usefulness. Recent work proving that highly strained multiferroic films of SrMnO₃ can be grown²³ is promising regarding the experimental verification of these results, while similar studies on Ba-doped systems^{30,37,38} would also be of interest. Further insights could also be obtained by studies using other computational methods, e.g., based on microscopic models for coupled spin-lattice dynamics^{39,40}.

Acknowledgments - A.E. is grateful to Quentin Meier for discussions. This work was supported by the Swiss National Science Foundation (project code 200021E-162297) and the German Science Foundation under the priority program SPP 1599 (“Ferroic Cooling”). Computational work was performed on resources provided by the Swiss National Supercomputing Centre (CSCS).

-
- ¹ S. Fähler, U. K. Rössler, O. Kastner, J. Eckert, G. Eggeler, H. Emmerich, P. Entel, S. Müller, E. Quandt, and K. Albe, *Advanced Engineering Materials* **14**, 10 (2012).
 - ² X. Moya, S. Kar-Narayan, and N. D. Mathur, *Nature Materials* **13**, 439 (2014).
 - ³ E. Stern-Taulats, T. Castán, L. Mañosa, A. Planes, N. D. Mathur, and X. Moya, *MRS Bulletin* **43**, 295 (2018).
 - ⁴ M. M. Vopson, *Solid State Communications* **152**, 2067 (2012).
 - ⁵ H. Meng, B. Li, W. Ren, and Z. Zhang, *Physics Letters A* **377**, 567 (2013).
 - ⁶ S. Anand and U. V. Waghmare, *Materials Research Express* **1**, 045503 (2014).
 - ⁷ A. Planes, T. Castan, and A. Saxena, *Philosophical Magazine* **94**, 1893 (2014).
 - ⁸ S. Lisenkov, B. K. Mani, C.-M. Chang, J. Almand, and I. Ponomareva, *Phys. Rev. B* **87**, 224101 (2013).
 - ⁹ Y. Liu, G. Zhang, Q. Li, L. Bellaiche, J. F. Scott, B. Dkhil, and Q. Wang, *Phys. Rev. B* **94**, 214113 (2016).
 - ¹⁰ Y.-Y. Gong, D.-H. Wang, Q.-Q. Cao, E.-K. Liu, J. Liu, and Y.-W. Du, *Advanced Materials* **27**, 801 (2015).
 - ¹¹ J. Liu, T. Gottschall, K. P. Skokov, J. D. Moore, and O. Gutfleisch, *Nature Materials* **11**, 620 (2012).
 - ¹² E. Mendive-Tapia and T. Castán, *Phys. Rev. B* **91**, 224421 (2015).
 - ¹³ Y. Liu, L. C. Phillips, R. Mattana, M. Bibes, A. Barthélémy, and B. Dkhil, *Nature Communications* **7**, 11614 EP (2016), article.
 - ¹⁴ T. Gottschall, A. Gràcia-Condal, M. Fries, A. Taubel, L. Pfeuffer, L. Mañosa, A. Planes, K. P. Skokov, and O. Gutfleisch, *Nature Materials* **17**, 929 (2018).
 - ¹⁵ N. A. Spaldin, S.-W. Cheong, and R. Ramesh, *Physics Today* **63**, 38 (2010).
 - ¹⁶ N. A. Spaldin and R. Ramesh, *Nature Materials* **18**, 203 (2019).
 - ¹⁷ We use the terminology of Ref. [7], that a multicaloric effect is the result of applying/removing multiple fields, additional to the sum of applying/removing each field separately. The caloric response in one ferroic property due to the field conjugate to another ferroic property coupled to the first one is called a cross-caloric effect.
 - ¹⁸ L. D. Landau, E. M. Lifshitz, and L. P. Pitaevskii, *Statistical Physics - Part 1*, 3rd ed., 10, Vol. 4 (Pergamon Press, Oxford, England, 1980).

- ¹⁹ A. Edström and C. Ederer, *Phys. Rev. Materials* **2**, 104409 (2018).
- ²⁰ J. H. Lee and K. M. Rabe, *Phys. Rev. Lett.* **104**, 207204 (2010).
- ²¹ C. Becher, L. Maurel, U. Aschauer, M. Lilienblum, C. Magé, D. Meier, E. Langenberg, M. Trassin, J. Blasco, I. P. Krug, P. A. Algarabel, N. A. Spaldin, J. A. Pardo, and M. Fiebig, *Nature Nanotechnology* **10**, 661 (2015), letter.
- ²² R. Guzman, L. Maurel, E. Langenberg, A. R. Lupini, P. A. Algarabel, J. A. Pardo, and C. Magen, *Nano Letters* **16**, 2221 (2016).
- ²³ J. W. Guo, P. S. Wang, Y. Yuan, Q. He, J. L. Lu, T. Z. Chen, S. Z. Yang, Y. J. Wang, R. Erni, M. D. Rossell, V. Gopalan, H. J. Xiang, Y. Tokura, and P. Yu, *Phys. Rev. B* **97**, 235135 (2018).
- ²⁴ T. Takeda and S. Ohara, *Journal of the Physical Society of Japan* **37**, 275 (1974).
- ²⁵ J. H. Lee and K. M. Rabe, *Phys. Rev. B* **84**, 104440 (2011).
- ²⁶ S. Kamba, V. Goian, V. Skoromets, J. Hejtmánek, V. Bovtun, M. Kempa, F. Borodavka, P. Vaněk, A. A. Belik, J. H. Lee, O. Pacherová, and K. M. Rabe, *Phys. Rev. B* **89**, 064308 (2014).
- ²⁷ E. O. Wollan and W. C. Koehler, *Physical Review* **100**, 545 (1955).
- ²⁸ See Supplemental Material at [URL will be inserted by publisher] for a detailed discussion regarding the determination of the parameters for the Landau theory.
- ²⁹ We note that the difficulty in treating ME coupling with only lowest order terms might also have important implications for other methods describing coupled dynamics between spin and lattice degrees of freedom, such as, e.g., described in Ref. [40].
- ³⁰ H. Sakai, J. Fujioka, T. Fukuda, D. Okuyama, D. Hashizume, F. Kagawa, H. Nakao, Y. Murakami, T. Arima, A. Q. R. Baron, Y. Taguchi, and Y. Tokura, *Phys. Rev. Lett.* **107**, 137601 (2011).
- ³¹ G. Giovannetti, S. Kumar, C. Ortix, M. Capone, and J. van den Brink, *Phys. Rev. Lett.* **109**, 107601 (2012).
- ³² The precise critical exponents would of course be altered in a theory correctly considering fluctuations.
- ³³ H. Wiegmann, A. G. M. Jansen, P. Wyder, J.-P. Rivera, and H. Schmid, *Ferroelectrics* **162**, 141 (1994).
- ³⁴ J. Íñiguez, *Phys. Rev. Lett.* **101**, 117201 (2008).
- ³⁵ A. Grünebohm, Y.-B. Ma, M. Marathe, B.-X. Xu, K. Albe, C. Kalcher, K.-C. Meyer, V. V. Shvartsman, D. C. Lupascu, and C. Ederer, *Energy Technology* **6**, 1491 (2018).
- ³⁶ A. Togo and I. Tanaka, *Scripta Materialia* **108**, 1 (2015).
- ³⁷ H. Somaily, S. Kolesnik, J. Mais, D. Brown, K. Chapagain, B. Dabrowski, and O. Chmaissem, *Phys. Rev. Materials* **2**, 054408 (2018).
- ³⁸ L. Maurel, N. Marcano, E. Langenberg, R. Guzmán, T. Prokscha, C. Magén, J. A. Pardo, and P. A. Algarabel, *APL Materials* **7**, 041117 (2019).
- ³⁹ I. A. Kornev, S. Lisenkov, R. Haumont, B. Dkhil, and L. Bellaiche, *Phys. Rev. Lett.* **99**, 227602 (2007).
- ⁴⁰ J. Hellsvik, D. Thonig, K. Modin, D. Iuşan, A. Bergman, O. Eriksson, L. Bergqvist, and A. Delin, *Phys. Rev. B* **99**, 104302 (2019).